ORAL/POSTER REFERENCE: ICF 100443OR

THERMAL-ELASTIC-PLASTIC COUPLED ANALYSES OF DYNAMIC CRACK GROWTH

F.Xu[1] W.Guo[1,2] Y.Y.Liu[3]
[1] State Key Laboratory of Mechanical Structure Strength and Vibration,
Xi'an Jiaotong University, 710049, Xi'an, PR China
[2]School of Aeronautics and Astronautics,
Nanjing University of Aeronautics and Astronautics, 210016, Nanjing, PR China
[3]Department of Aircraft Engineering,
Northwestern Polytechnical University, 710072, Xi'an, PR China

ABASTRACT

Finite Element Analyses (FEA) on dynamic crack growth with different velocity have been conducted on the basis of a strain rate thermal-elastic-plastic coupled model for an aluminum alloy. The dynamic J integral and recently developed incremental path-independent T^* integral are studied and the T^* integral is shown to be a more reasonable parameter in characterizing dynamic crack growth. Although the crack tip stresses and plastic strain decrease with increasing crack growth velocity, the triaxiality stress parameter is nearly unchanged in front of a moving tip. Fluctuant expansion of plastic strain zone for different growing velocities appears in the analyses. Through the cases studied here, the effect of temperature rise on the crack tip field is weaker than that of the strain rate.

KEYWORDS

thermal-elastic-plastic, strain rate, dynamic fracture, incremental path independent integral, temperature rise, crack growth, crack tip fields, triaxiality stress

INTRODUCTION

Dynamic fracture mechanics is a main offshoot of fracture mechanics and considers the effects of inertia of material element and strain rate. Due to the high strain rate near the dynamic crack tip, temperature rise is inevitable which makes the problem more complex and better understanding is necessary.

The J integral has received much attention in monotonic nonlinear fracture mechanics as it can characterize the near tip asymptotic fields. Unfortunately, in company with unloading in crack growth, the theoretical foundation of the J integral does not permit further extension of its utility. Some more reasonable integrals based on the incremental plastic theory have been proposed in recent years. The T^* integral presented by Altluri [1,2] has been developed and found application in a wide range of problems [3,4,5]. Experimental methods to measure the T^* integral have also been developed [6].

Previous works have demonstrated that the temperature rise caused by plastic deformation is significant in some cases. However, simulating model suitable for this phenomenon has not been well established [7,8]. Because the strain rate is very high at the crack tip of high velocity crack propagation, which would affect the yield stress immediately, this factor must be taken into account as well [9,10].

Consequently, this paper focuses on the coupled effect of temperature and strain rate on dynamic crack growth. The J integral and T^* integral are evaluated on the basis of finite element analyses and crack tip

stresses, strains, triaxiality stress and plastic zone are discussed.

ANALYTICAL MODEL

Dependence of the yield stress on temperature and strain rate

Based on micro scale energy transformation analyses in ductile materials, two models among yield stress σ_{ys}, temperature T and strain rate $\dot{\varepsilon}$ are proposed [11] as in the following.

$$\sigma_{ys} = \sigma_a + \sigma_p^*[1 - \frac{kT\ln(A/\dot{\varepsilon})}{\Delta H_0}]^n , \tag{1}$$

$$\sigma_{ys} = \sigma_a + \sigma_p^*[\frac{1 - kT\ln(A/\dot{\varepsilon})}{\Delta H_0}] \quad . \tag{2}$$

where the σ_a is internal stress and stands for non-temperature part, σ_p^* is the equivalent stress under absolute zero temperature, k is Bossman constant. Once the material constants A, σ_a and ΔH_0 are determined, yield stress can be evaluated.

Constitutive relations on the coupled effect of temperature and strain rate

A widely used empirical relationship between yield stress and strain rate is prescribed as [12,13]

$$\sigma = \sigma_G(\varepsilon, T = T_0)[1 - \beta(T - T_0)]\left(\frac{\dot{\varepsilon}_p}{\dot{\varepsilon}_0}\right)^m , \qquad m<<1. \tag{3}$$

where $\dot{\varepsilon}_0$ is the reference strain rate, T_0 is the reference temperature, σ_G is the yield stress under the reference strain rate, m and β are material constants. In this paper, material constants m and β are determined to be 0.005 and 0.001 by a lot of experimental results for a thin plate aluminum alloy. Recently, the above equation has been used in the study of micro scale dynamic fracture [14].

When the strain rate increases up to a certain value, the heat transformed from the plastic work cannot be exchanged with the environment, which then causes the temperature rise. The temperature rise during the adiabatic process can be calculated from the viewpoint of energy balance as

$$\Delta T = \frac{\chi}{\rho C_p}\int \sigma_{ij} d\varepsilon_{ij}^p \quad . \tag{4}$$

where ρ and C_p are the density and the specific heat of a material. χ is heat transformation coefficient, which has been demonstrated to be great than 90% for large amount of metal materials once the crack growing velocity is higher than *100m/s* [7,14].

NUMERICAL PROCEDURE

Finite element model and method

The basic geometry of a compact tension (CT) specimen is as follows: length equals 120mm, width equals 110mm, thickness equals 2.8mm and crack length equals 55mm. Only one half of the model is established for the symmetric geometry. About 700 four-node elements are used in the mesh and the minimum element length is 0.25mm. Distributed force is applied to the loading hole. In order to simulate the crack growth well, spring element is used in the ligament.

Fixed mesh method is used to simulate the crack growth in this paper. In order to avoid the sudden jump during the growing process, at every crack increment, i.e. the minimum element length, the node constraint is released for several sub-steps by using the spring elements.

Practical use of the T^* integral parameter

The physical interpretations of the T^* integrals for the circle path or the Dugdale path are different. [1,2] T^* evaluated along a Dugdale path is interpreted as the energy flow into a finite-sized process zone. Dugdale path is chosen here for the sake of the application of the node constraint releasing technique. The features that T^* evaluated along the Dugdale path converges to a finite value, and it is independent on mesh size, are very helpful.

In practical operation, it is easy to perform the calculation by

$$T^*\Big|_{\varepsilon} = T^*\Big|_{\varepsilon=0} - \int_{V_\varepsilon} [W_{,1} - (\sigma_{ij}\varepsilon_{ij,1})]dV \,, \tag{5}$$

$$T^*\Big|_{\varepsilon=0} = \int_{\Gamma_f} [Wn_1 - t_i u_{i,1}]d\Gamma + \int_{V_f} [W_{,1} - (\sigma_{ij}\varepsilon_{ij,1})]dV \,. \tag{6}$$

where Γ_f is a path which circles the crack far from the crack tip, and V_f is the volume within Γ_f. ε is the size of finite buffer zone around the crack. It is convenient to evaluate the integrals using Eqn. 6, and then subtracts out the V_ε term.

RESULTS AND DISCUSSIONS

The J and T^* Integrals

The effect of different paths on the evaluated values of T^* integral is shown in Fig. 1, where the symbols *1,2,3,4,5* and *6* represent paths from the far field to the near tip field. It is obvious that the values of T^* integral are consistent for far-field path marked by *1,2* and *3*. Values of the T^* integral calculated from the middle-field path are the same as that of far-field path before the crack initiation and decrease a little during the crack propagation. Symbol *6* represents the most near-field path, which is only five or six times the minimum element length away from the tip. Since the influence of finite strain is significant in the near tip, the integral values deviate from the far-field one. In the following discussions the results of the far-field integral are used. The effect of buffer zone size ε on the T^* integral is also discussed. In the FE model, which is made of the four-node element, the buffer zone of two or three element length is suggested, which is similar to that of the eight-node element.

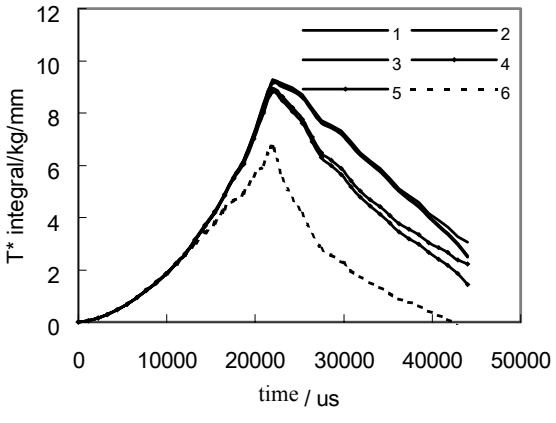

Figure 1: The effect of different paths to T^* integral

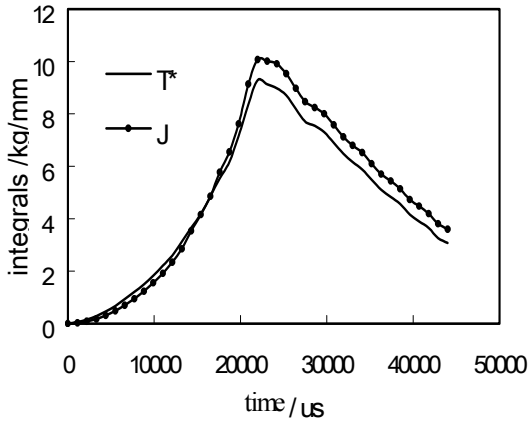

Figure 2: Comparison between the two integrals

Figure 2 shows a basic feature between the T^* integral and dynamic J integral under the crack growing velocity of *0.3m/s*. The two integrals are consistent, with T^* value being a little smaller than J value. These give the meaning that under the condition of low strain rate, small crack growth, isothermal and isotropic material, monotonic loading, dynamic J integral can be extended to control crack growth for a certain length. Through the analyses of two typical stress states, it is shown that dynamic J integral is of the ability to

control a longer crack length in the state of plane stress than in plane strain.

Figure 3(a) shows T^* integral for five different crack growing velocities. It can be found that the integral decreases as crack growing velocity or growing length increases. The tendency of the T^* integral to the growing velocity is more disciplinary than that of the J integral. Further comparisons between T^* integral and dynamic J integral for different crack growing velocities are shown in Fig. 3(b). When the crack growing velocity is *100m/s*, T^* integral and J integral are consistent for a length after the crack initiate. When the growing velocity increases to *500m/s*, the consistent length is much shorter. When the growing velocity reaches up to *1000m/s*, dynamic J integral is useless. These two groups of curves are not shown for the limited space, but can be found in the reference [15]. It is very interesting that when the growing velocity is *2000m/s*, the two integrals approach again. This phenomenon can be explained by the strong effect of the inertia and stress wave under dynamic condition. The high growing velocity obviously reduces the plastic unloading zone, so the J integral is useful again. Since it is really hard for metals to reach such a crack growing velocity as *2000m/s,* generally speaking, the J control zone decreases as the crack growing velocity increases.

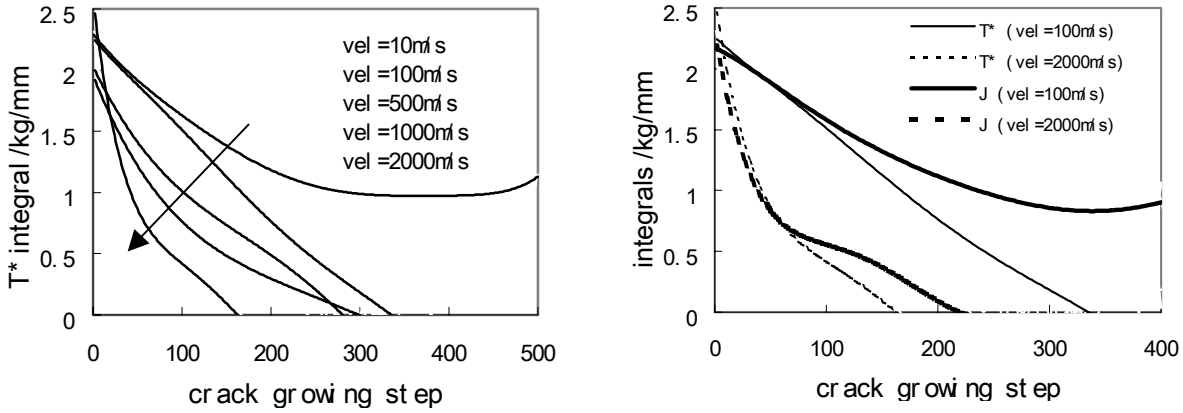

(a) T^* integral (b) J integral

Figure 3: Comparison of integrals for different growing velocity

The effect of temperature rise and strain rate on the integral parameters are shown in table 1. The subscript '*c*' stands for the reference case in which neither temperature nor strain rate is thought of. The subscript '*t*' represents the case that only temperature effect is taken into account. The subscript '*s*' stands for the case that both temperature and strain rate are considered. It can be seen from the table that the T_t^* is slightly smaller than the T_c^*, while the J_t is nearly the same as J_c. This means that the T^* integral is more sensitive to the changes at the crack tip than the J integral. T_s^* and J_s are obviously higher than their reference values in case '*c*'. This illustrate that the effect of the strain rate is much stronger than that of temperature rise in the present calculation.

TABLE 1

THE EFFECT OF TEMPERATURE AND STRAIN RATE ON THE INTEGRAL PARAMETERS

Growing velocity *m/s*	Jc *kg/mm*	Jt *kg/mm*	Js *kg/mm*	Tc^* *kg/mm*	Tt^* *kg/mm*	Ts^* *kg/mm*
500	.847	.849	.872	.486	.480	.589
1000	.277	.277	.304	.118	.111	.142
2000	.370	.370	.895	.169	.157	.778

(The growing length simulated by FEA is 30mm for the velocities 500m/s and 1000m/s and 10mm for velocity 2000m/s.)

The stress and strain fields

The study of the crack tip fields is a very important aspect in the fracture mechanics. Since there is no theoretical solution for the open mode elastic-plastic dynamic crack tip fields, the study of the distribution of stresses, strains and other relevant parameters in front of a moving crack tip is essential.

Figure 4 shows the distributions of open stress σ_{yy}, equivalent plastic strain ε_p and triaxiality stress $R_\sigma = \sigma_m / \sigma_e$ in the front of a growing crack at velocity *1000m/s*. The initial position of the crack tip is located at the coordinates *(20,0)*. The crack growing direction is along the positive of the *X* direction. The symbols *1,2,3,4* and *5* represent different crack growing length *2mm, 6mm, 10mm, 14mm* and *18mm* respectively. In order to explain the features of the high velocity crack growing process thoroughly, the stable elastic-plastic crack propagation and the low velocity crack propagation are discussed at the same time, although the results are not shown. (See reference [15].) It can be seen from Fig. 4(a) that the maximum values are stable in crack growing process with high velocity. In contrast, for stable elastic-plastic crack propagation, open stress increases as the crack grows. Although the equivalent plastic strain increases for stable and low velocity crack growth, it decreases during the high velocity crack propagation, as shown in Fig. 4(b). This is due to the delay in development of plastic strain under high strain rate. From Fig. 4(c), a regular pattern can be seen that the triaxiality stress keeps constant for a certain distance in front of a growing crack tip, which exists in all cases of stable, low velocity and high velocity crack propagations. Compared with different growing velocities *100m/s, 500m/s* and *2000m/s*, it can be learned that the stress and strain both decrease when the growing velocity increase, while the maximum triaxiality stress is nearly independent of growing velocity, with the high triaxiality stress region reducing with the growing velocity.

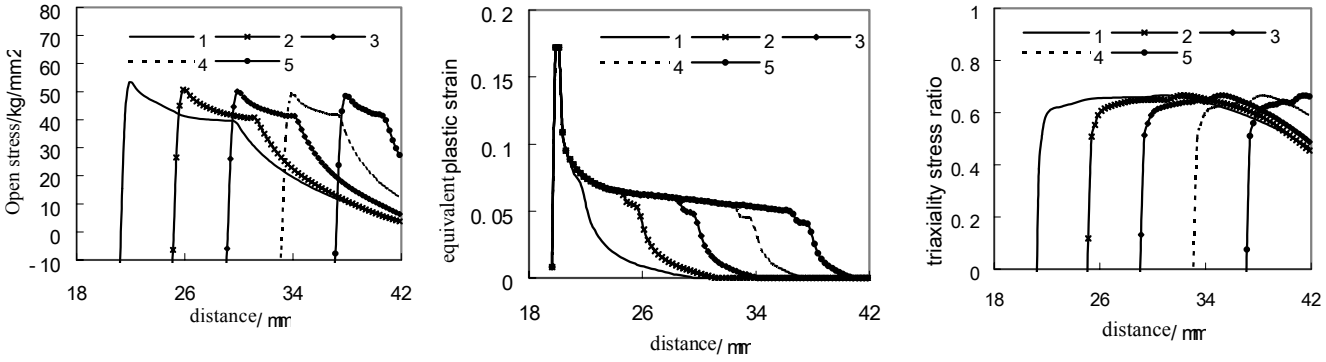

(a) open stress (b) equivalent plastic strain (c) triaxiality stress

Figure 4: The distribution of stress and strain during the crack propagation

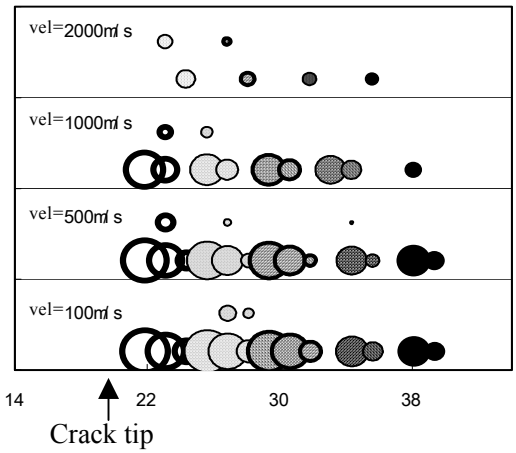

Figure 5: The evolvement of the plastic zone at different growing velocity

Figure 5 shows the evolvement of the plastic zone at different growing velocities, *100m/s, 500m/s, 1000m/s* and *2000m/s* respectively. Five crack growing lengths *2mm, 6mm, 10mm, 14mm* and *18mm* are shown by five types of circles, where the crack initiates at the coordinates of *20mm* on the axis of abscissas. The size of a circle represents the value of the plastic strain and the center of a circle gives the location of the strain. It is obvious that the plastic zone reduces monotonously under high growing velocity, while it firstly increases then decreases under moderate growing velocity. In the case of stable elastic-plastic crack propagation, a monotonous size increment of plastic zone is found.

The effect of the temperature rise and the strain rate on the growing crack tip field is discussed in detail. For the material and the loading condition considered here, the plastic zone is small, then the temperature rise is only *10℃* for a growing velocity, while the temperature drop deduced by the high strain rate is *78℃*. So we can say again that the effect of the strain rate on the crack tip field is stronger than that of the temperature.

CONCLUSIONS

The T^* integral is more reasonable in the analyses for dynamic crack growth than the J integral, while the dynamic J integral can be extended to control crack growth under certain conditions.

When the crack growing velocity increases, both the stress and the strain at the crack tip decrease, while the triaxiality stress keeps constant in front of the moving crack tip.

When the effects of the temperature and strain rate are taken into account of, it can be found that the strain rate will more strongly affect the crack tip field than the temperature.

The plastic zone evolves monotonously under both stable crack growth and high growing velocity propagation, which expands in the former and shrinks in the latter. Under a moderate growing velocity, the plastic zone increases at first, and then reduces.

REFERENCE

1. Brust, F.W., Nishioka, T. and Altluri, S.N. etc. (1985) *Engng. Fracture Mech.* 22(6), 1079-1103.
2. Altluri, S.N. and Nishioka, T. (1984) *Engng. Fracture Mech.* 20(2), 209-244.
3. Brust, F.W. and Altluri, S.N. (1986) *Engng. Fracture Mech.* 23(3), 551-574.
4. Liu, C.D., Han, Y.F. and Yan, M.G. (1992) *Engng. Fracture Mech.* 43(5), 827-836.
5. Xu, F., Guo, W. and Liu, Y.Y. (2000) *Chinese J. of Applied Mech*. 40(4), 102-106
6. Okada, H., Atluri, S.N. and Omori, Y. (1999) *J. of Plasticity* 15, 869-897
7. Kuang, Z.B and Altluri, S.N. (1985) *J. of Applied Mech*., Trans. ASTM 52, 274-280.
8. Zehnde, A.T. and Rosakis, A.J. (1991) *J. Mech. Phys. Solid,* 39(3), 385-415.
9. Rice, J.R. and Levy, N. (1969). In: *Physics of strength and plasticity*, MIT, Cambridge, 227-293.
10. Kallivayalil, J.A., Hui, C.Y. and Zehnder, A.T. (1996) *Int. J. solids and structures*, 33(13), 1867-1889.
11. Lie, W.S., Yan, M. and Chen, B.S. (1996) *Engng. Fract. Mech.*, 53(4),633-643.
12. Pan, J., Saje, M. and Needleman, A. (1984) *Acta. Metal.* 32,157-169.
13. Needlimam, A. and Tvergaard, V. (1991) *Int. J. Fract.*, 49,41-67.
14. Sun, D.Z. and Honig, A. etc. (1995) *ASTM STP 1220*, 343-357.
15. Xu, F. (1998). *DSc Thesis*, Northwestern Polytechnical University, China.